Long-term homeostatic T cell proliferation is driven by AMPK-dependent regulation of oxygen reactive species

Anouk Lepez[1]*, Tiphène Pirnay[1]*, Sébastien Denanglaire[1], David Perez-Morga[2,3], Marjorie Vermeersch[2], Oberdan Leo[1]* and Fabienne Andris[1]*[$]

[1] Laboratory of Immunobiology, Université Libre de Bruxelles, Belgium

[2] Center for Microscopy and Molecular Imaging (CMMI), Université Libre de Bruxelles, Belgium

[3] Laboratory of Molecular Parasitology, Université Libre de Bruxelles, Belgium

Running Title: AMPK regulates homeostatic T cell proliferation

* *co-first or co-last authors*

[$] *correspondence should be addressed to:*

Dr. Fabienne Andris, Laboratoire d'Immunobiologie, Université Libre de Bruxelles – IBMM, 12, rue des Prof. Jeener et Brachet, 6041 Gosselies, BELGIUM

tel : +32 2 650 9880 ; fax: +32 2 650 9860 ; email : fandris@ulb.ac.be

Key words: T lymphocytes, cell metabolism, homeostasis, ROS, GVHD

Abstract

Under lymphopenia, fast proliferation of peripheral lymphocytes, driven by the availability of interleukin-7 and the engagement of the T cell receptor, results in a large pool of effector/memory T cells that may potentiate anti-tumor immunotherapies but also lead to auto-immune complications.

Naïve, effector and memory CD4 T lymphocytes display particular energy metabolism and it has been shown that fine-tuning of cell metabolism might govern T cell differentiation. However, whether T cell metabolism controls homeostatic proliferation is unknown. Here, we report that deficiency in the energy sensor metabolic enzyme AMP-activated kinase (AMPK) results in reduced accumulation of effector/memory T cells during the course of homeostatic proliferation. Accordingly, hematopoietic stem cell transplantation of AMPK-deficient T cells into allogeneic recipient led to a reduced graft-versus-host disease. Moreover, we show that AMPK expression enhances the mitochondrial potential of T cells, limits reactive oxygen species (ROS) production, and resolves ROS-mediated toxicity. Dampening ROS production alleviates the proliferative defect of AMPK-deficient T cells, therefore indicating a role for an AMPK-mediated ROS control of homeostatic proliferation.

Introduction

The size of the T cell pool is maintained by a combination of T cell production by the thymus and by the gradual turnover of mature T cells in the periphery. This mature T cell proliferation is regulated by a limited supply of interleukin 7 (IL-7) as well as TCR signals and is part of a process by which the immune system reinstates the homeostatic balance (1–3).

In response to lymphopenia induced by irradiation, chemotherapy or viral infection, residual naive T cells undergo augmented homeostatic proliferation. Similarly, the adoptive transfer of small numbers of naive T cells into syngeneic lymphopenic host results in their robust expansion of the transferred T cells. These highly proliferative donor T cells acquire memory cell surface markers, express effector functions and have been shown to provide protective immunity against bacterial infection (4–8).

T cells undergoing homeostatic expansion during allogeneic hematopoietic stem cell transplantation (HSCT) also contribute to the new host memory T cell pool and can lead to a significant graft-versus-tumor (GVT) protective effect (9). However, HSCT is also often associated with the development of immunopathology resulting from uncontrolled donor T cell activation that can lead to fatal adverse reactions defined as graft-versus-host diseases (GVHD) (10).

Changes in the proliferative and functional state of T lymphocytes during an immune response are accompanied by profound modifications in the cell metabolism. Whereas naive T cells generate the largest part of their ATP through mitochondrial oxidative phosphorylation (OxPhos), activated lymphocytes rely heavily on glycolysis to fulfill their energetic demands (11, 12). Long-lived memory T cells that subsist after primary infection convert back to an oxidative metabolism with a marked preference for fatty acid as primary energy source (FAO) (11, 13).

T cell-specific deletion of the apoptosis inducing factor (AIF), a mitochondrial inter-membrane space protein required for efficient assembly of the complex I of the electron transport chain, leads to defective homeostatic proliferation, suggesting that T cell homeostatic proliferation also relies on active mitochondrial function (14). Accordingly, in a semi-allogeneic model of GVHD, pharmacological blockade of fatty acid oxidation decreased the survival of transferred T cells and alleviated the severity of the disease (15). However, using two different models of GVHD, Nguyen et al reported that glycolysis was required for

optimal function of alloantigen-activated T cells and inhibition of glycolysis by targeting mTORC1 or 6-phosphofructo-2-kinase/fructose-2,6-biphosphatase 3 (PFKFB3) ameliorated GVHD mortality and morbidity (16, 17). It is also possible that T cells balance their metabolism between active glycolysis and oxidative phosphorylation to sustain homeostatic proliferation, as shown for T cell acute lymphoblastic leukemia cells (18).

The AMP-activated protein kinase (AMPK) maintains the energy balance in eukaryotic cells and is a central regulator of cellular responses to metabolic stress (19–21). Activation of AMPK decreases fatty acid and protein synthesis (22, 23), and promotes FAO and mitochondrial biogenesis (24, 25). AMPK also up-regulates the rate of glycolysis through phosphorylation of PFKFB3 and increased glucose uptake (26, 27).

The transition of proliferative effector $CD8^+$ T lymphocytes to quiescent memory T cells during the contraction phase of the immune response to *Listeria monocytogenes* infection has been linked to the activation of AMPK (28). Although AMPK is activated early during T cell primary responses *in vitro* and *in vivo* (13, 29), two independent studies reported that AMPK was dispensable for the generation of effector T cells (28, 30). However, effector T cells lacking AMPKα1 displayed reduced mitochondrial bioenergetics and cellular ATP in response to glucose limitation, in support of a role for AMPK in the metabolic adaptations of activated effector T cells (31).

AMPK also recently emerged as an important sensor and regulator of mitochondrial ROS and a regulator of ROS neutralization by antioxidant cellular systems, thereby maintaining adequate cellular oxidative balance (32). Yet a role for AMPK in the control of ROS production and sensitivity has not been described for T cells.

Here we show that AMPK promotes long-term T cell proliferation and effector functions upon transfer of T cells into lymphopenic recipients and during the course of a GVHD reaction. AMPK-deficient T cells respond to IL-7 survival signaling but show decreased mitochondrial potential, enhanced ROS production, and increased susceptibility to ROS-mediated toxicity. Dampening ROS production partly restores the homeostatic proliferation of AMPK-deficient T cells, suggesting a role for an AMPK/mitochondria/ROS-driven pathway in this process.

Results

1. AMPK promotes effector / memory T cells engraftment in the peripheral tissues of bone marrow chimeras

To investigate the role of AMPK in T cell homeostasis, we used conditional KO mice in which loxP-flanked alleles of AMPKα1 (prkaa1$^{f/f}$) are deleted by the Cre recombinase expressed from the CD4^{+} T-cell-specific Cd4 promoter (prkaa1$^{f/f}$ - CD4-Cre mice, hereafter referred as AMPK^{KO-T} mice). No major abnormalities in the thymic and splenic lymphoid populations of these mice have been reported (28, 30). To evaluate whether expression of AMPK modulates the size of T cell compartments in a homeostatic competitive environment, we generated chimeras by reconstituting irradiated CD3ε$^{-/-}$ recipient mice with a 1:1 mixture of congenitally marked bone marrow cells from wild type (CD45.1^{+}) and AMPK^{KO-T} (CD45.2^{+}) donor mice. The average contribution of WT and AMPK-KO cells to the repopulation of the thymus, spleen and lymph nodes CD4 and CD8 T cell compartments was comparable (Figure 1A, B). Of interest, AMPK-KO splenocytes expressed significantly lower percentage of CD44^{hi} CD62L^{low} surface markers characteristic of effector / memory cells (Figure 1C-F). The AMPK-KO T cell compartment was also markedly deficient in the expression of the tissue homing CXCR3 chemokine receptor (Figure 1G, H). Accordingly, T cells derived from AMPK^{KO-T} mice contributed only marginally to the repopulation of the gut lymphoid tissues when compared to wild type T cells three months after competitive bone marrow transplantation (Figure 1A, B and supplemental Fig S1A). A reduced reconstitution of the AMPK-KO T cell pool was also observed in the liver of chimeras (supplemental Figure S1B). Thus, AMPK is required for T cells to properly exit from naive "progenitor" state and could provide a competitive advantage to effector / memory phenotype T cells in engrafting the niche of non-hematopoietic tissues following adoptive transfer of bone marrow precursors in T cell deficient mice.

2. AMPK promotes T cell homeostatic proliferation and confers higher pathogenicity to donor T cells during GVHD

To further study homeostatic T cell proliferation of AMPK-KO CD4^{+} T cells, we used the well-established model of lymphopenic mice, in which the proliferation of naive CD4^{+} T cells is driven predominantly by IL-7 availability and by weak interactions with self-peptide/MHC complexes as well as microbial-derived antigens (33). CFSE-labeled, congenitally marked, CD44^{low} CD4^{+} T cells were purified from WT and AMPK^{KO-T} mice and co-transferred into CD3ε$^{-/-}$ lymphopenic recipient mice. Ten days after adoptive transfer, splenic CD4^{+} T cells

expressing high and low CFSE contents, respectively indicative of slow and fast homeostatic proliferation, were recovered in both both WT and AMPK-KO subsets. As expected, fast divided cells up-regulated CD44 expression (Figure 2C and supplemental Figure S2A). Despite starting with similar number of cells, the recovery of donor WT $CD4^+$ T cells was reproductively greater than that of AMPK-KO cells in each organ tested (Figure 2A, B). Co-transfer of naive B6.CD45.1 and B6.CD45.2 (both WT genotype) led to similar $CD4^+$ T cell recovery, indicating that CD45 polymorphism does not affect homeostatic proliferation of T lymphocytes (supplemental Figure S3A, B). Of interest, subdivision of splenic $CD4^+$ T cell populations based on CFSE content indicated that the relative contribution of AMPK-KO cells to the T cell pool decreased over T cell divisions (Figure 2C, D; see also supplemental Figure S2B for individual mouse representation). The lower percentage of AMPK-KO T cells undergoing fast division rates is further reflected by their lower expression of the Ki67 proliferation marker (Figure 2E). Wild type fast dividing cells acquired potential for IFNγ secretion as well as cell surface expression of CXCR3 (Figure 2F, H, upper panels: compare 0-2 and 3 division groups). Both CXCR3 expression and IFNγ secretion were significantly reduced in the AMPK-KO subset whereas comparable IL-2 secretion was observed in WT and KO groups (Figure 2F-J).

Similar results were obtained following homeostatic proliferation of *in vitro*-derived memory-like Th1 cells (see supplemental Figure S4 for details). Moreover non-divided WT and AMPK-KO Th1 cells were recovered at similar frequencies upon transfer into lymphoreplete C57BL6 mice, suggesting that AMPK-KO T cells did not experience increased cell death *in vivo* (supplemental Figure S4B).

To further assess if AMPK promotes *in vivo* proliferation in a non-competitive model and sustains T cell pathogenicity during GVHD, we transferred wild type or AMPK-KO T cells ($H\text{-}2^b$), together with wild type T-depleted bone marrow precursors, into lethally irradiated Balb/c ($H\text{-}2^d$) recipient mice. Decreased percentages of allogeneic $CD4^+$ were recovered from the spleen of recipient mice transplanted with AMPK-KO T cells (Figure 3A). Although the proportion of allogeneic Tregs was very low in this experimental setting, we observed a significant increase in their frequencies in AMPK-KO transplants (Figure 3B). No difference was observed in allogeneic $CD8^+$ T cells frequency (Figure 3C). Futhermore GVHD clinical score was decreased in recipients of AMPK-KO T cells (Figure 3D). Accordingly, WT T cells caused rapid lethality in almost all the recipients, whereas AMPK-KO T cells only caused lethality in a fraction of the recipients (Figure 3E), thus suggesting that AMPK activation is

required to induce T cell pathogenicity and GVHD.

AMPK is dispensable for IL-7 and TCR early signaling but required for optimal T cell expansion *in vitro*

WT and AMPK-KO naive T cells expressed similar levels of phospho-STAT5 and phospho-STAT1 in response to IL-7 and survived, for at least 14 days, in IL-7-supplemented media (supplemental Figure S5 and data not shown).

To further study the role of AMPK in the homeostatic expansion of $CD4^+$ T cells, we developed an *in vitro* model of T cell proliferation in the presence of autologous dendritic cells and IL-7, based on a recent report of Rosado-Sánchez et al (34). Two weeks *in vitro* culture of CFSE-labeled naive Th cells with autologous DCs and IL-7, but not DCs or IL-7 alone, led to T cell expansion, characterized by increased cell number recovery and the presence of both slow and fast divided cells (see Supplemental Figure S6 for details). As previously observed *in vivo*, only fast dividing cells acquired $CD44^{hi}$ / $CD62L^{low}$ effector cell marker expression and secrete IFNγ (Supplemental Figure S6D). Although a 14-day culture in IL-7-containing media already resulted in a small decrease in the AMPK-KO Th cell recovery, the DC+IL-7-driven homeostatic proliferation (HP) resulted in a further gradual decrease over time (Figure 4A, B). Accordingly, KO/WT cell ratio was further decreased among fast divided ($CFSE^{low}$) cells (Figure 4C, D). Similar results have been observed with memory-like Th1 subjected to homeostatic proliferation *in vitro* (Figure 4F). As previously shown in the *in vivo* model, AMPK-KO Th cells secreted less IFNγ, compared to their wild type counterparts (Figure 4E).

In agreement with our previous report (30), AMPK-KO naive T cells expressed early T cell activation markers and displayed normal short-term TCR-dependent proliferative response to anti-CD3 or allogeneic APCs (supplemental Figure S7A-C). However, co-culture of WT and AMPK-KO T cell in the presence of anti-CD3/CD28 mAbs revealed a small decrease in the AMPK-KO versus WT Th cell recovery. Futhermore WT Th cells largely outcompete their AMPK-KO counterparts when further expanded with IL-2 (supplemental Figure S7D). Collectively, these data indicate that AMPK sustains prolonged cytokine-driven T cell proliferation and/or viability.

AMPK regulates mitochondrial fitness in T cells

RNA-seq analysis revealed no difference in the pattern of gene expression between WT and KO Th cells recovered from DC + IL-7 cultures (Supplemental Figure S8), indicating a negligible role of AMPK in the regulation of gene transcription in this experimental setting.

We next sought to investigate whether AMPK would be implicated in the mitochondrial bioenergetic functions of IL-7-driven homeostatic proliferating T cells (either in the DC + IL-7 HP model or in the asynchronous anti-CD3 + IL-7 memory-like Th1 model). In both models, AMPK-KO Th cells displayed similar mitochondrial mass (Mito-Green staining) but expressed reduced mitochondrial membrane potential, as judged by both TMRE and JC-1 staining (Figure 5A-C). Freshly purified (or rested in IL-7 supplemented media) AMPK-KO naïve Th cell already expressed a slight reduced mitochondrial membrane potential (Figure 5D). Although AMPK-KO T cells recovered after 14 days of homeostatic proliferation exhibited a severe decrease in their mitochondrial membrane potential, this was not associated with changes in oxygen consumption rate (OCR) or extra-cellular acidification rate (ECAR) (Figure 5E-G and Figure S9). Transmission electron microscopy (TEM) revealed that AMPK-KO T cells did not show difference in mitochondria size and number (Figure 5H-J). Yet we noticed an increased percentage of mitochondria harboring localized increased membrane density and membrane budding in AMPK-KO cells (Figure 5K, L).

Turnover of damaged mitochondria is part of the mitochondrial quality control process and it has recently been shown that enhanced mitophagy can slow-down the cell cycle progression (35). To measure mitochondria turnover in IL-7-treated WT and AMPK-KO Th cells cultures, we pulsed-chased mitochondria with the Mito-Green Traker probe and followed the Mito-Green loss over time. We chose to perform these experiments on non-dividing IL-7-treated naïve Th cells to avoid interferences between mitochondria turnover (on a per cell basis) and mitochondria dilution over cell divisions. As a control, cells were re-stained with the mitochondrial probe at each timing to check for total mitochondrial content. As shown in Figure 6A, B, Mito-Green staining gradually decreased over time and AMPK-KO Th cells exhibited increased mitochondrial turnover at each time point.

Mitochondrial fitness is essential for the rapid induction of glycolysis during re-activation of memory CD8+ T cells (36). Interestingly, WT but not AMPK-KO Th cells recovered from IL-7-driven HP or memory-like cultures showed increased ECAR upon both mitochondria stress and anti-CD3 / CD28 re-stimulation (Figure 6C, D and supplemental Figure S9D).

Dampening ROS production partially restores the competitive proliferative capacity of AMPK-KO T cells

Mitochondria are major cellular sources of reactive oxygen species (ROS) (37, 38). In agreement with a role for AMPK in maintaining redox balance in cancer cells (39, 40), AMPK-KO homeostatic proliferating T cells and memory-like Th1 cells generated increased amounts of ROS (Figure 7B, C). Although freshly purified or IL-7 cultured AMPK-KO naïve Th cells expressed similar levels of intra-cellular ROS at steady state (compare Figure 7A and B), they were highly sensitive to ROS-mediated cell death (Figure 7D), further indicating that AMPK regulates ROS balance and protects Th cells from ROS-mediated toxicity. WT and AMPK-KO Th cells exhibited similar sensitivity to a pro-apoptotic drug staurosporine (Figure 7 E), confirming the selectivity of AMPK for ROS-driven cell death. Similar results were obtained with memory Th1-like cells (Supplemental Figure S10).

Whereas low concentrations of ROS are essential for T cell activation and proliferation, high concentration of ROS affect cell survival, thereby highlighting a major role for anti-oxidative processes in the tight control of intra-cellular ROS equilibrium and cell proliferation (41). To test whether increased ROS levels expressed by AMPK-KO Th cells would impede their competitive proliferation, we set up homeostatic proliferation cultures in the absence or presence of antioxidants. In agreement with our working hypothesis, lack of 2-mercaptoethanol (2-ME), a potent reducing agent that prevents toxic levels of oxygen radicals through stabilization of the intracellular cysteine and GSH levels (42, 43), led to a reduced proliferative capacity of AMPK-KO when compared to WT cells (Figure 7F, G). Accordingly, supplementation of the culture media with the ROS scavenger MitoTEMPO reduced intra-cellular ROS contents and partially restored the proliferative competence of AMPK-KO Th cells (Figure 7H, I).

Materials and methods

Mouse model

AMPK$\alpha 1^{fl/fl}$ mice were kindly provided by Dr. B. Viollet (Institut Cochin, Paris - France) and bred to CD4-Cre transgenic mice, obtained from Dr. G. Van Loo (University of Gand - Belgium). C57BL/6 and Balb/c mice were purchased from Envigo (Horst - Nederland). CD45.1 were purchased from Jackson Laboratory (Bar Harbor - USA) and CD3$\varepsilon^{-/-}$ were

obtained from EMMA (Orléans – France). Control mice were littermate AMPKα1$^{fl/fl}$ Cre^{-} or AMPKα1$^{+/fl}$ Cre^{-} or sex- and age-matched C57BL/6 or CD45.1 mice. Mice were housed under specific pathogen-free (SPF) conditions. The experiments were performed in compliance with the relevant laws and institutional guidelines and were approved by the Local Ethic Committee.

Cell purifications

Bone marrow cells from tibia and femur were purified from naive mice by flushing. When required (GVHD), T cells were magnetically depleted. Briefly, bone marrow cells were incubated 20 min at 4°C with anti-CD4 (L3T4)-, anti-CD8α (Ly-2)- and anti-CD90.2-MicroBeads (Miltenyi Biotec, Bergisch-Gladbach, Germany) and then separated over an auto-MACS column using the DepleteS program.

Total T cells (CD4^{+} and CD8^{+}) were purified from the spleen of naive mice by Stemcell negative selection, according to manufacturer's recommendations. Briefly, spleen cells were incubated 30 min at 4°C with 0,5 µg/ml of anti-Ter119-biot (Ly-76), anti-CD19-biot (MB19-1), anti-Gr1-biot (RB6-8C5), anti-CD49b-biot (DX5), anti-CD11c-biot (N418) and anti-MHCII (I-A/I-E)-biot (M5/114) antibodies. Antibodies are from BD Biosciences or BioXCell. Cells were then incubated with Biotin selection cocktail 2 (Stemcell) for 17 min at 4°C. D2 Magnetic Particles (Stemcell) were added and cells were incubated for an additional 7 min at 4°C before placing them in the Stemcell magnet.

Naive T cells (CD4^{+} CD44^{-}) were purified from the spleen of naive mice by MACS column enrichment followed by cells sorting. Spleen cells were incubated at 4°C with anti-CD4 (L3T4)-MicroBeads (Miltenyi Biotec) after 10 min CD4 (RM4-5)-PB, CD44 (IM7)-PE-Cy7, CD62L (MEL-14)-A700 and CD25 (PC61)-BB515 were added for an additional 15 min. These antibodies are all from BD. The cells were first separated over an LS-column (Miltenyi Biotec) and the CD4^{+} fraction was then sorted as CD4^{+} CD25^{-} CD62L^{+} CD44^{-} by FACS ARIA III (BD Biosciences).

For dendritic cell purification, spleens were treated with collagenase (Gestimed). Recovered splenocytes were resuspended in Nicodenz (DO_{360}=0.666, Lucron Bioproducts). RPMI-medium with 3% FCS was added on the top of Nicodenz. After 15 min centrifugation at 4°C and 1700G without brake, DC fraction were recovered from the gradient interface and incubated with CD11c-MicroBeads (Miltenyi Biotec) for 15 min at 4°C. The excess of beads was washed out and cells were then separated over an LS-column (Miltenyi Biotec).

Bone marrow transfer

Bone marrow cells purified from WT (CD45.1) and AMPK^{KO-T} (CD45.2) mice were mixed at ratio 1:1 and i.v. injected (4 to 5.10^6 cells in total) into 1200 cGy (split dose) irradiated CD3ε$^{-/-}$ mice. 8 to 12 weeks later, WT and AMPK-KO T cells from different organs were analyzed by flow cytometry.

***In vivo* homeostatic proliferation**

Naive (CD4$^+$ CD44$^-$) cells obtained from WT (CD45.1) and WT or AMPK^{KO-T} (CD45.2) mice were mixed at ratio 1:1 and i.v. injected (1-2.10^6 cells in total) into CD3ε$^{-/-}$ mice. 10 to 12 days later, WT and AMPK-KO T cells from different organs are analyzed by flow cytometry. In some experiments cells were CFSE-labelled (Invitrogen) before i.v. injection.

GVHD

Irradiated Balb/c mice (750 cGy, day -1) were i.v. injected with 5.10^6 C57BL/6 T cell depleted bone marrow with or without 10^6 total T cells from either WT or AMPK^{KO-T} mice (day 0). Clinical score was followed three times a week and calculated as previously described by Cooke et al, 1996 (44). 7 to 10 days later, WT and AMPK-KO T cells from different organs are analyzed by flow cytometry.

Isolation of intestinal lymphocytes

Intestines were collected and cleared from residual connective tissue, Peyer's patches and feces. Intestines were then cut into small pieces and incubated for 30 min at 37°C with agitation in a medium containing EDTA (2.5 mM, VWR) and DTT (72.5 µg/ml, Sigma-Aldrich). IEL were recovered by washing and shaking the intestines 3 times in a medium with EDTA and one time without EDTA. To obtain LP lymphocytes, intestines were further chopped and incubated for 30 min at 37°C in medium containing liberase (20 µg/ml, Roche) and DNAse (400 µg/ml, Roche). Enzymes were neutralized with EDTA (2.5 mM) and the intestines were crushed and filtered. IEL and LP fractions were finally washed and submitted to 15 min centrifugation at 500G, 20°C without break in a 30% Percoll (GE Healthcare) solution. Lymphocytes are in the pellet.

***In vitro* differentiation of memory-like Th cells**

Naive T cells (CD4$^+$ CD44$^-$) were polarized into Th1 cells for 3 days using plate-bound anti-CD3 (5 µg/ml, clone 145-2C11, BioXCell), anti-CD28 (1 µg/ml, clone 37.51, BioXCell), recombinant IL-12 (10 ng/ml, Peprotech) and anti-IL-4 (10 µg/ml, BioXCell). Th1 cells were then cultured, for 4 to 7 additional days, into IL-7-supplemented (20 ng/ml, Peprotech) media to obtain memory-like cells.

***In vitro* homeostatic proliferation**

Naive T cells ($CD4^+$ $CD44^-$) purified from WT (CD45.1) and $AMPK^{KO-T}$ (CD45.2) mice were mixed at a 1:1 ratio, CFSE-labelled and seeded in a 96-well plate (10^5 cell/well). T cells were cultured at 37°C in RPMI supplemented with 5% heat-inactivated FBS (Sigma-Aldrich), 1% non-essential amino acids (Invitrogen), 1 mM sodium pyruvate (Invitrogen), 2 mM L-glutamin (Invitrogen), 500 U/mL penicillin/500 µg/ml streptomycin (Invitrogen), and 50 µM β-mercaptoethanol (Sigma-Aldrich). The homeostatic stimuli were provided by 2.10^4 DC purified from autologous C57BL/6 (H-2^b) mice and IL-7 (20 ng/ml, Peprotech). Each 4-5 days of culture, half of the medium volume was refreshed with new IL-7-supplemented medium and freshly purified DC. Cells were analyzed on day 13-15. For antioxidant supplementation, MitoTEMPO (20 µM, Sigma) was added to culture medium and refreshed at the same time than IL-7.

Memory-like Th1 from WT (CD45.1) and $AMPK^{KO-T}$ (CD45.2) mice were mixed at ratio 1.1 and were cultured with 2.10^4 syngeneic DC and IL-7 (20 ng/ml, Peprotech) for 9 additional days. Half of the medium volume was refreshed with new IL-7-supplemented medium and freshly purified DC at day 5.

Flow cytometry

Specific cell-surface staining was performed using standard procedure with the following monoclonal antibodies conjugated to fluorochrome or biotin: CD4 (RM4-5), CD44 (IM7), CD45.1 (A20) from BD Bioscience, and CD8α (53-6.7), CD183 (CXCR3-173), CD62L (MEL-14), TcRβ (H57-597) from eBioscience. Strepatividin was purchased from BD Bioscience. Dead cells were excluded by LIVE/DEAD (Invitrogen) staining and non-specific, Fc-mediated interactions were blocked by anti-Mouse CD16/CD32 (2.4G2 BioXCell). For intracellular staining, cells were incubated with a fixing solution (Fixation/Permeabilization, eBioscience) and stained with directly conjugated monoclonal antibodies anti-IFNγ (XMG1.2), IL-2 (JES6-5H4), Ki67 (B56) from BD-Bioscience, and FoxP3 (FJK-16s) from eBioscience. For cytokine production assessment, cells were pre-incubated for 4 h with PMA 50 ng/ml (Sigma), ionomycin 1 µg/ml (Sigma) and brefeldin A (eBiosciences).

For mitochondrial parameters analysis, cells were incubated 25 min at 37°C with the Mito-Green dye (100 nM, Invitrogen), TMRE (5 nM, Invitrogen) or JC-1 probe (2 µM, Invitrogen) in complete medium.

For the mitochondria renewal assay, naïve T cells were stained with Mito-Green dye (2 µM, Invitrogen) for 20 min at 37°C (10^6 cells per 100 µL). Then the loss of this staining was

recorded by flow cytometry at day 4, 6 and 9. At each time point, fresh staining of Mito-Green dye was performed to measure total mitochondria content on unstained cells (100 nM).

For ROS detection, cells were incubated 30 min at 37°C with Dihydrorhodamine (DHR) 123 (2 µM, Sigma) in complete medium.

Cells were analyzed by FACS Canto II or ARIA III (BD Bioscience) and data were analyzed with the FlowJo Software (Tree Star).

Seahorse

OCR and ECAR were determined using a Seahorse XFp or XF96 Extracellular Flux Analyser following user guide. Plate were pre-coated with poly-D-lysine (200 µg/ml, Millipore) for cell adhesion. 1 mM pyruvate, 2 mM de glutamine and 10 mM glucose were added to XF Base Medium and pH was adjusted to 7.4. Drugs were added to reach a final concentration of: oligomycin 1 µM, FCCP 0.5 µM, rotenone/antimycin A 0.5µM and 2-DG 50mM. For CD3/CD28 beads (Dynabeads Mouse T-Activator CD3/CD28, LifeTechnologies) injection, beads:cells ratio was 4:1. Seahorse protocol was adjusted with the following settings: mix 2min, wait 2min and measure 4-5min. At the end of the Seahorse analysis, cells were lysed and Bradford (Biorad) protein dosage was performed.

ROS / staurosporine-sensitivity

2-5.10^5 cells were incubated for 2 h with different concentrations of H_2O_2 (Merck) or for 2, 4 or 6 h with staurosporine (5 µg/ml, Sigma) at 37°C. The percentage of survival was measured after Propidium iodide staining (Sigma).

Transmission Electron Microscopy (TEM)

A total of 27 (WT) and 29 (AMPK-KO) T cells were analyzed by transmission electron microscopy. Naïve T cells were maintained 4 days in IL-7-supplemented medium and then fixed overnight in 2.5% glutaraldehyde (Electron Microscopy Sciences, UK) at 4°C and post-fixed with 1% osmium tetroxide (Electron Microscopy Sciences, UK) and 1,5 % ferrocyanide (Electron Microscopy Sciences, UK) in 0,15 M cacodylate buffer. The cells were further stained with 1% uranyl acetate (Electron Microscopy Sciences, UK), serially dehydrated and embedded in epoxy resin (Agar 100 resin; Agar Scientific, UK). Ultrathin 70-nm sections were produced with a Leica EM UC6 ultramicrotome and mounted on copper–Formvar–carbon grids (Electron Microscopy Sciences). Observations were made on a Tecnai 10 electron microscope (FEI, Eindhoven, Netherlands), and images were captured with a Veleta camera and processed with SIS iTEM sofware (Olympus, Germany).

Statistical analysis

Statistical analysis were performed using Prism6 (GraphPad Software, San Diego, CA). Datasets were first tested for Gaussian distribution with the D'Agostino & Pearson omnibus normality test. Statistical analysis performed are detailed for each graph in the figure legend. n.s.: non significant; *p < 0,05; **p< 0,01; ***p< 0,001; ****p< 0,0001.

References

1. Sprent J, Surh CD. 2011. Normal t cell homeostasis: the conversion of naive cells into memory-phenotype cells. *Nat. Immunol.* 131(6):478–84
2. Min B, Yamane H, Hu-Li J, Paul WE. 2005. Spontaneous and homeostatic proliferation of cd4 t cells are regulated by different mechanisms. *J. Immunol.* 174(10):6039–44
3. Min B. 2018. Spontaneous t cell proliferation: a physiologic process to create and maintain homeostatic balance and diversity of the immune system. *Front. Immunol.* 9:547
4. Cho BK, Rao VP, Ge Q, Eisen HN, Chen J. 2000. Homeostasis-stimulated proliferation drives naive t cells to differentiate directly into memory t cells. *J. Exp. Med.* 192(4):549 LP – 556
5. Stephan O, Karin B. 2006. Naïve cytotoxic t lymphocytes spontaneously acquire effector function in lymphocytopenic recipients: a pitfall for t cell memory studies? *Eur. J. Immunol.* 29(2):608–14
6. Haluszczak C, Akue AD, Hamilton SE, Johnson LDS, Pujanauski L, et al. 2009. The antigen-specific cd8⁺ t cell repertoire in unimmunized mice includes memory phenotype cells bearing markers of homeostatic expansion. *J. Exp. Med.* 206(2):435 LP – 448
7. Hamilton SE, Wolkers MC, Schoenberger SP, Jameson SC. 2006. The generation of protective memory-like cd8+ t cells during homeostatic proliferation requires cd4+ t cells. *Nat. Immunol.* 7:475
8. Goldrath AW, Bogatzki LY, Bevan MJ. 2000. Naive t cells transiently acquire a memory-like phenotype during homeostasis-driven proliferation. *J. Exp. Med.* 192(4):557 LP – 564
9. Dummer W, Niethammer AG, Baccala R, Lawson BR, Wagner N, et al. 2002. T cell homeostatic proliferation elicits effective antitumor autoimmunity. *J. Clin. Invest.* 110(2):185–92
10. Pidala J. 2011. Graft-vs-host disease following allogeneic hematopoietic cell transplantation. *Cancer Control*. 18(4):268–76
11. Chang C-H, Pearce EL. 2016. Emerging concepts of t cell metabolism as a target of immunotherapy. *Nat. Immunol.* 17:364
12. Vander Heiden MG, Cantley LC, Thompson CB. 2009. Understanding the warburg effect: the metabolic requirements of cell proliferation. *Science (80-.).* 324(5930):1029 LP – 1033

13. Pearce EL, Walsh MC, Cejas PJ, Harms GM, Shen H, et al. 2009. Enhancing cd8 t-cell memory by modulating fatty acid metabolism. *Nature*. 460(7251):103–7

14. Milasta S, Dillon CP, Sturm OE, Verbist KC, Brewer TL, et al. 2016. Apoptosis-inducing-factor-dependent mitochondrial function is required for t cell but not b cell function. *Immunity*. 44(1):88–102

15. Byersdorfer CA, Tkachev V, Opipari AW, Goodell S, Swanson J, et al. 2013. Effector t cells require fatty acid metabolism during murine graft-versus-host disease. *Blood*. 122(18):3230 LP – 3237

16. Nguyen HD, Chatterjee S, Haarberg KMK, Wu Y, Bastian D, et al. 2016. Metabolic reprogramming of alloantigen-activated t cells after hematopoietic cell transplantation. *J. Clin. Invest.* 126(4):1337–52

17. Nguyen HD, Kuril S, Bastian D, Yu X-Z. 2018. T-cell metabolism in hematopoietic cell transplantation

18. Kishton RJ, Barnes CE, Nichols AG, Cohen S, Gerriets VA, et al. 2016. AMPK is essential to balance glycolysis and mitochondrial metabolism to control t-all cell stress and survival. *Cell Metab.* 23(4):649–62

19. Hardie DG, Ross FA, Hawley SA. 2012. AMPK: a nutrient and energy sensor that maintains energy homeostasis. *Nat. Rev. Mol. Cell Biol.* 13(4):251–62

20. Andris F, Leo O. 2014. AMPK in lymphocyte metabolism and function. *Int. Rev. Immunol.* 1:67–81

21. Ke R, Xu Q, Li C, Luo L, Huang D. 2017. Mechanisms of ampk in the maintenance of atp balance during energy metabolism. *Cell Biol. Int.* 42(4):384–92

22. Inoki K, Zhu T, Guan K-L. 2003. TSC2 mediates cellular energy response to control cell growth and survival. *Cell*. 115(5):577–90

23. Hardie DG, Pan DA. 2002. Regulation of fatty acid synthesis and oxidation by the amp-activated protein kinase. *Biochem. Soc. Trans.* 30(6):1064 LP – 1070

24. Jäger S, Handschin C, St.-Pierre J, Spiegelman BM. 2007. AMP-activated protein kinase (ampk) action in skeletal muscle via direct phosphorylation of pgc-1α. *Proc. Natl. Acad. Sci.* 104(29):12017 LP – 12022

25. Fullerton MD, Galic S, Marcinko K, Sikkema S, Pulinilkunnil T, et al. 2013. Single phosphorylation sites in acc1 and acc2 regulate lipid homeostasis and the insulin-sensitizing effects of metformin. *Nat. Med.* 19:1649

26. Marsin A-S, Bouzin C, Bertrand L, Hue L. 2002. The stimulation of glycolysis by hypoxia in activated monocytes is mediated by amp-activated protein kinase and inducible 6-phosphofructo-2-kinase. *J. Biol. Chem.* . 277(34):30778–83

27. Fryer LGD, Foufelle F, Barnes K, Baldwin SA, Woods A, Carling D. 2002. Characterization of the role of the amp-activated protein kinase in the stimulation of glucose transport in skeletal muscle cells. *Biochem. J.* 363(1):167 LP – 174

28. Rolf J, Zarrouk M, Finlay DK, Foretz M, Viollet B, Cantrell DA. 2013. AMPKα1: a glucose sensor that controls cd8 t-cell memory. *Eur. J. Immunol.* 43(4):889–96

29. Tamás P, Hawley SA, Clarke RG, Mustard KJ, Green K, et al. 2006. Regulation of the energy sensor amp-activated protein kinase by antigen receptor and ca2+ in t lymphocytes. *J. Exp. Med.* 203(7):1665–70

30. Mayer A, Denanglaire S, Viollet B, Leo O, Andris F. 2008. AMP-activated protein kinase regulates lymphocyte responses to metabolic stress but is largely dispensable for immune cell development and function. *Eur. J. Immunol*. 38(4):948–56

31. Blagih J, Coulombe F, Vincent EE, Dupuy F, Galicia-Vázquez G, et al. 2015. The energy sensor ampk regulates t cell metabolic adaptation and effector responses in vivo. *Immunity*. 42(1):41–54

32. Rabinovitch RC, Samborska B, Faubert B, Ma EH, Gravel SP, et al. 2017. AMPK maintains cellular metabolic homeostasis through regulation of mitochondrial reactive oxygen species. *Cell Rep*. 21(1):1–9

33. Boyman O, Krieg C, Homann D, Sprent J. 2012. Homeostatic maintenance of t cells and natural killer cells. *Cell. Mol. Life Sci*. 69(10):1597–1608

34. Rosado-Sánchez I, González-Magaña A, Pozo-Balado MM, Herrero-Fernández I, Polaino MJ, et al. 2018. An in vitro system of autologous lymphocytes culture that allows the study of homeostatic proliferation mechanisms in human naive cd4 t-cells. *Lab. Investig*. 98(4):500–511

35. Sarraf SA, Sideris DP, Giagtzoglou N, Ni L, Kankel MW, et al. 2019. PINK1/parkin influences cell cycle by sequestering tbk1 at damaged mitochondria, inhibiting mitosis. *Cell Rep*. 29(1):225-235.e5

36. van der Windt GJW, O'Sullivan D, Everts B, Huang SC-C, Buck MD, et al. 2013. CD8 memory t cells have a bioenergetic advantage that underlies their rapid recall ability. *Proc. Natl. Acad. Sci. U. S. A.* 110(35):14336–41

37. Turrens JF. 2003. Mitochondrial formation of reactive oxygen species. *J. Physiol*. 552(Pt 2):335–44

38. Sena LA, Li S, Jairaman A, Prakriya M, Ezponda T, et al. 2013. Mitochondria are required for antigen-specific t cell activation through reactive oxygen species signaling. *Immunity*. 38(2):225–36

39. Zhao Y, Hu X, Liu Y, Dong S, Wen Z, et al. 2017. ROS signaling under metabolic stress: cross-talk between ampk and akt pathway. *Mol. Cancer*. 16:79

40. Jeon S-M, Chandel NS, Hay N. 2012. AMPK regulates nadph homeostasis to promote tumour cell survival during energy stress. *Nature*. 485(7400):661–65

41. Mak TW, Grusdat M, Duncan GS, Dostert C, Nonnenmacher Y, et al. 2017. Glutathione primes t cell metabolism for inflammation. *Immunity*. 46(4):675–89

42. Ishii T, Bannai S, Sugita Y. 1981. Mechanism of growth stimulation of l1210 cells by 2-mercaptoethanol in vitro. role of the mixed disulfide of 2-mercaptoethanol and cysteine. *J. Biol. Chem.* . 256(23):12387–92

43. Ishii T, Mann GE. 2014. Redox status in mammalian cells and stem cells during culture in vitro: critical roles of nrf2 and cystine transporter activity in the maintenance of redox balance. *Redox Biol.* 2:786–94

44. Cooke KR, Kobzik L, Martin TR, Brewer J, Delmonte J, et al. 1996. An experimental model of idiopathic pneumonia syndrome after bone marrow transplantation: i. the roles of minor h antigens and endotoxin. *Blood*. 88(8):3230–39

Figure legends

<u>Figure 1</u>: AMPK promotes peripheral T cells replenishment upon bone marrow transfer

(**A-B**) Relative contribution of AMPK-KO $CD4^+$ (**A**) and $CD8^+$ (**B**) T cells in the thymus, spleen, MLN, LP and IEL of $CD3\varepsilon^{-/-}$ mice were reconstituted with a 1:1 mixture of bone marrow cells from WT (CD45.1) and $AMPK^{KO\text{-}T}$ (CD45.2) mice. Data are expressed as a ratio of AMPK-KO over WT cells in the $CD4^+$ or $CD8^+$ T cell gate. (**C-H**) CD62L, CD44 and CXCR3 expression by WT and AMPK-KO T cells recovered from the spleen of mice reconstituted as in (**A**, **B**). Representative dot plots (**C**, **E**) and histograms showing the mean % +/- SD (**D**, **F**) in different cell gates as indicated. Data are representative of 3 (**A**, **C**, **D**, **G**, **H**) or 2 (**B**, **E**, **F**) independent experiments with n = 6.

Statistical analysis: Friedman followed by Dunn multiple comparison (**A**, **B**), Mann–Whitney (**D**, **F**), Wilcoxon Test (**H**). * $p < 0.05$; ** $p < 0.01$; *** $p < 0.001$

<u>Figure 2:</u> WT $CD4^+$ T cells outcompete their AMPK-KO counterparts during homeostatic proliferation

CFSE labeled $CD4^+$ naive T cells from WT (CD45.1) and $AMPK^{KO\text{-}T}$ (CD45.2) mice (1:1 ratio) were i.v. injected into $CD3\varepsilon^{-/-}$ mice. Recovered T cells were analyzed on day 10 by flow cytometry.

(**A, B**) Relative contribution of AMPK-KO T cells to the repopulation of the $CD4^+$ T cell subset in the spleen, MLN, LP and IEL ($CD4^+$ gated). Representative dot plots (**A**) and histograms showing the ratio of AMPK-KO / WT cells (**B**, gate $CD4^+$ T cells). Data are representative of 3 (LP, IEL), 4 (MLN) or 6 (spleen) independent experiments with n=6. (**C**) CFSE dilution versus CD45.1 expression by $CD4^+$ T cells in the spleen. (**D**) Relative contribution of AMPK-KO T cells in the pool of recovered splenic $CD4^+$ T cells that divided 0-2 or > 3 times, according to CFSE dilution (pool of 4 independent experiments with n = 15). (**E**) Percentage of WT and AMPK-KO $CD4^+$ T cells that express Ki67 in the spleen (1 experiment representative of 2, with n = 5). (**F-H**) Percentage of WT and AMPK-KO $CD4^+$ T cells expressing CXCR3 (**F**) or producing IL-2 and IFNγ (**H**) according to the number of cell divisions in the spleen. (**G-J**) Percentage of WT and AMPK-KO $CD4^+$ T cells expressing CXCR3 (**G**), IL-2 (**I**) or IFNγ (**J**) among $CD4^+$ T cells that divided more than 3 times (pool of 2-3 independent experiments, with n = 7-10).

Statistical analysis: Friedman followed by Dunn multiple comparison (**B**), Wilcoxon (**D**, **E**, **G**, **I** and **J**). * $p < 0.05$; ** $p < 0.01$; *** $p < 0.001$, **** $p < 0.0001$

<u>Figure 3:</u> Knock-down of AMPK in donor T cells decreases the severity of GVHD

(**A**-**C**) Percentage of allogenic $CD4^+$ (**A**) Tregs (**B**) and $CD8^+$ (**C**) T cells in the spleen of the Balb/c host mice.

Data are pooled from 5 independent experiments with a total n = 26 (WT group) and 27 (AMPK-KO group). Clinical score (**D**) and survival (**E**) of host mice (n = 8 per group, 1 experiment representative of 3).

Statistical analysis: Mann–Whitney (**A-D**), Mantel-Cox (**E**). * $p < 0.05$; ** $p < 0.01$; *** $p < 0.001$

<u>Figure 4:</u> AMPK promotes homeostatic proliferation *in vitro*

(A) Relative recovery of AMPK-KO T cells after 14 day-culture with IL-7 in the presence or absence of syngenic DC. (**B**) Relative recovery of AMPK-KO T cells at day 6 and 14 of IL-7+DC culture. (**C**) CFSE dilution profiles of WT and AMPK-KO at day 14 of IL-7+DC culture. (**D**) Relative contribution of AMPK-KO T cells according to CFSE content. (**E**) Percentage of WT and AMPK-KO T cells expressing IFNγ at day 14. (**F**) Relative recovery of AMPK-KO memory-like Th1 cells after a 9 day-homeostatic culture with IL-7 and syngeneic DCs.

Data are representative of at least 5 experiments with n = 17 (**A**) or 8 (**B**), or are pool of 2 independent experiments with n = 13 (**D**) or 11 (**E**).

Statistical analysis: Mann–Whitney (**A**), Friedman followed by Dunn multiple comparison (**B**) Wilcoxon (**D**-**F**). * $p < 0.05$; ** $p < 0.01$; **** $p < 0.0001$

<u>Figure 5:</u> AMPK promotes mitochondrial fitness of T cells

(**A**) Mitochondrial mass (Mito-Green, left panel) and mitochondrial membrane potential (TMRE, right panel) in WT and AMPK-KO memory-like Th1 cells. (**B**-**D**) Mitochondrial membrane potential measured as a ratio of JC1 Red/Green ratio in memory-like Th1 cells (**B**), in HP-recovered T cells (**C**) and in naïve T cells (**D**): FACS staining of a representative experiment and histogram showing the mean +/- SD of red/green fluorescence with WT ratio

set to 1. (**E-G**) Basal OCR (**E**), maximal OCR (**F**) and ECAR (**G**) of HP-recovered T cells. (**H-J**) TEM analysis of WT and AMPK-KO naïve T cells. Representative images (**H**), numbers (**I**) and areas (**J**) of mitochondria (a total of 179 (WT) and 170 (KO) mitochondria from 27 (WT) and 29 (AMPK-KO) T cells analyzed are represented. (**K, L**) Image representative (**K**) and percentage of mitochondria presenting a budding protrusion (WT : 3 out of 179, AMPK-KO : 16 out 170 mitochondria).

Data are representative of 3 (**A**), 7 (**C**, **D**) or 2 (**H**, **K**) experiments or are pooled from 9 (**B**) or 2 (**A-G**, n= 6) independent experiments.

Statistical analysis: paired t-test (**B-D**), Mann–Whitney (**E-G, I-J**), Chi^2 (**L**). ** $p < 0.01$; *** $p < 0.001$; **** $p < 0.0001$

<u>Figure 6:</u> Accelerated mitochondrial clearance and defective mitochondrial stress-induced glycolytic switch in AMPK-KO T cells

(**A**) Representative FACS profiles of total mitochondrial mass (left panel) and pulse-chase remaining mitochondrial staining (right panels) in WT and AMPK-KO T cells at day 4, 6 and 9 of HP. (**B**) Kinetic of mitochondrial mass loss, calculated from gate indicated in (**A**, right panels). (**C, D**) Kinetic of ECAR upon oligomycin treatment of WT and AMPK-KO Th1 memory-like cells (**C**) or HP-recovered T cells (**D**).

Data are pooled from 3 independent experiments (n = 9-16, **B**) or 2 independent experiments (n = 6, **D**), or are representative of 7 individual experiments (n = 16, **C**).

Statistical analysis: Wilcoxon (**B**), Mann-Withney (**C**, **D**). ** $p < 0.01$; *** $p < 0.001$; **** $p < 0.0001$

<u>Figure 7:</u> AMPK dampens ROS production and toxicity in T cells

(**A-C**) Cellular ROS staining with DHR123 probe in naïve T cells (**A**), in HP-recovered T cells (**B**), and in memory-like Th1 cells (**C**). FACS staining of a representative experiments (left panels) and histogram showing MFI fold increase in AMPK-KO cells in comparison to WT cells set to 1 (right panels). (**D, E**) Percentages of cell viability after treatement of WT and AMPK-KO naïve Th cells with H_2O_2 (0.5 mM for 2h, **D**) or with staurosporine (STS, 5 µM for 2h, **E**). (**F, H**) Cellular ROS staining of naïve Th cells after 4 days in IL-7 supplemented culture medium with or without 2-ME (**F**) and supplemented with MitoTEMPO (**H**). (**G, I**) Relative recovery of AMPK-KO T cells after 14 days of homeostatic proliferation *in vitro* in a culture medium with or without 2-ME (**G**) and with or without MitoTEMPO (**I**).

Data are pooled from 7 (n = 7, **A**), 9 (n = 11, **B**), (n = 8, **C**), 3 (n = 5, **D**), 4 (n = 4, **E**), 4 (n = 20, **G**) or 6 (n = 13, **I**) independent experiments or are representative of 3 individual experiments (**F**, **H**). Statistical analysis: Wilcoxon (**A-C**), Mann–Whitney (**D, E, G, I**). * $p < 0.05$; ** $p < 0{,}01$; **** $p < 0{,}0001$

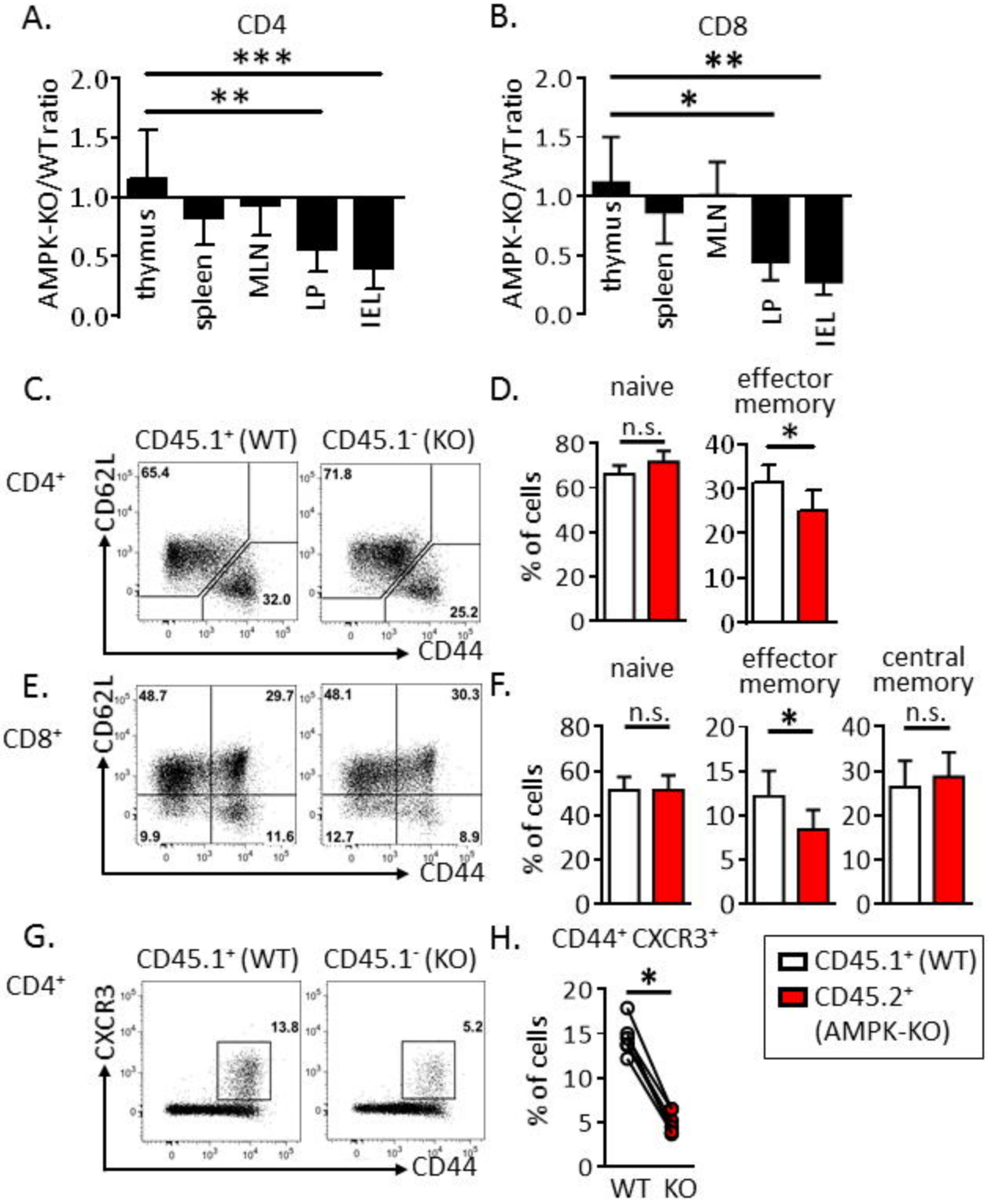
A.
CD4
***
**
AMPK-KO/WT ratio
2.0
1.5
1.0
0.5
0.0
thymus
spleen
MLN
LP
IEL
B.
CD8
**
*
AMPK-KO/WT ratio
2.0
1.5
1.0
0.5
0.0
thymus
spleen
MLN
LP
IEL
C.
CD45.1+ (WT)
CD45.1- (KO)
CD4+
CD62L
65.4
32.0
71.8
25.2
CD44
D.
naive
effector memory
n.s.
*
% of cells
80
60
40
20
0
40
30
20
10
0
E.
CD8+
CD62L
48.7
29.7
9.9
11.6
48.1
30.3
12.7
8.9
CD44
F.
naive
effector memory
central memory
n.s.
*
n.s.
% of cells
80
60
40
20
0
20
15
10
5
0
40
30
20
10
0
G.
CD45.1+ (WT)
CD45.1- (KO)
CD4+
CXCR3
13.8
5.2
CD44
H.
CD44+ CXCR3+
*
% of cells
20
15
10
5
0
WT
KO
CD45.1+ (WT)
CD45.2+ (AMPK-KO)

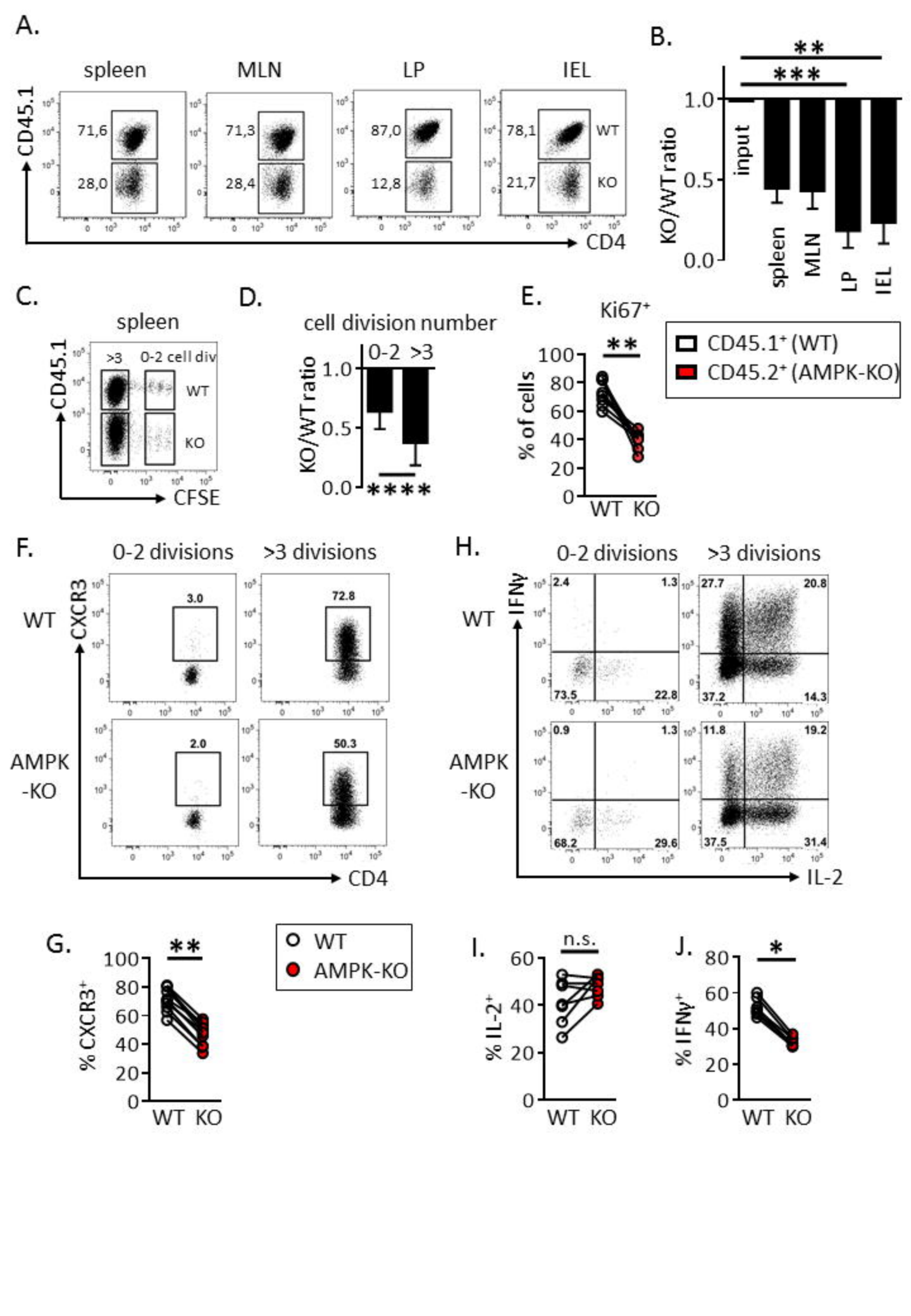
A.
spleen
MLN
LP
IEL
CD45.1
CD4
71,6
28,0
71,3
28,4
87,0
12,8
78,1
21,7
WT
KO
B.
KO/WT ratio
1.0
0.5
0.0
input
spleen
MLN
LP
IEL
**
***
C.
spleen
CD45.1
CFSE
>3
0-2 cell div
WT
KO
D.
cell division number
KO/WT ratio
0-2
>3
****
E.
Ki67+
% of cells
**
WT
KO
CD45.1+ (WT)
CD45.2+ (AMPK-KO)
F.
0-2 divisions
>3 divisions
WT
AMPK -KO
CXCR3
CD4
3.0
72.8
2.0
50.3
H.
0-2 divisions
>3 divisions
WT
AMPK -KO
IFNγ
IL-2
2.4
1.3
73.5
22.8
27.7
20.8
37.2
14.3
0.9
1.3
68.2
29.6
11.8
19.2
37.5
31.4
G.
% CXCR3+
**
WT
KO
WT
AMPK-KO
I.
% IL-2+
n.s.
WT
KO
J.
% IFNγ+
*
WT
KO

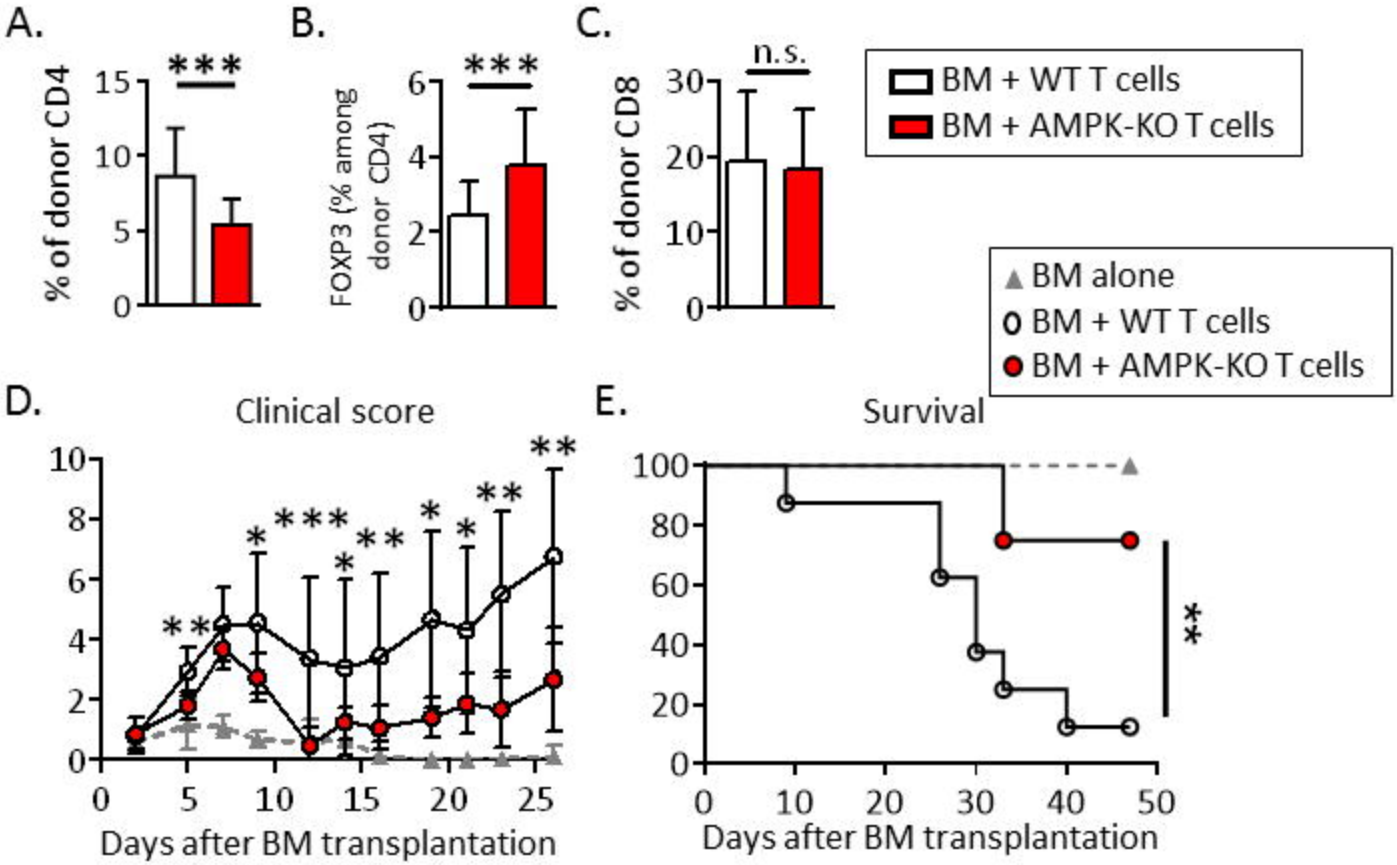
A.
B.
C.
% of donor CD4
FOXP3 (% among donor CD4)
% of donor CD8
***
***
n.s.
BM + WT T cells
BM + AMPK-KO T cells
BM alone
BM + WT T cells
BM + AMPK-KO T cells
D.
Clinical score
Days after BM transplantation
E.
Survival
Days after BM transplantation

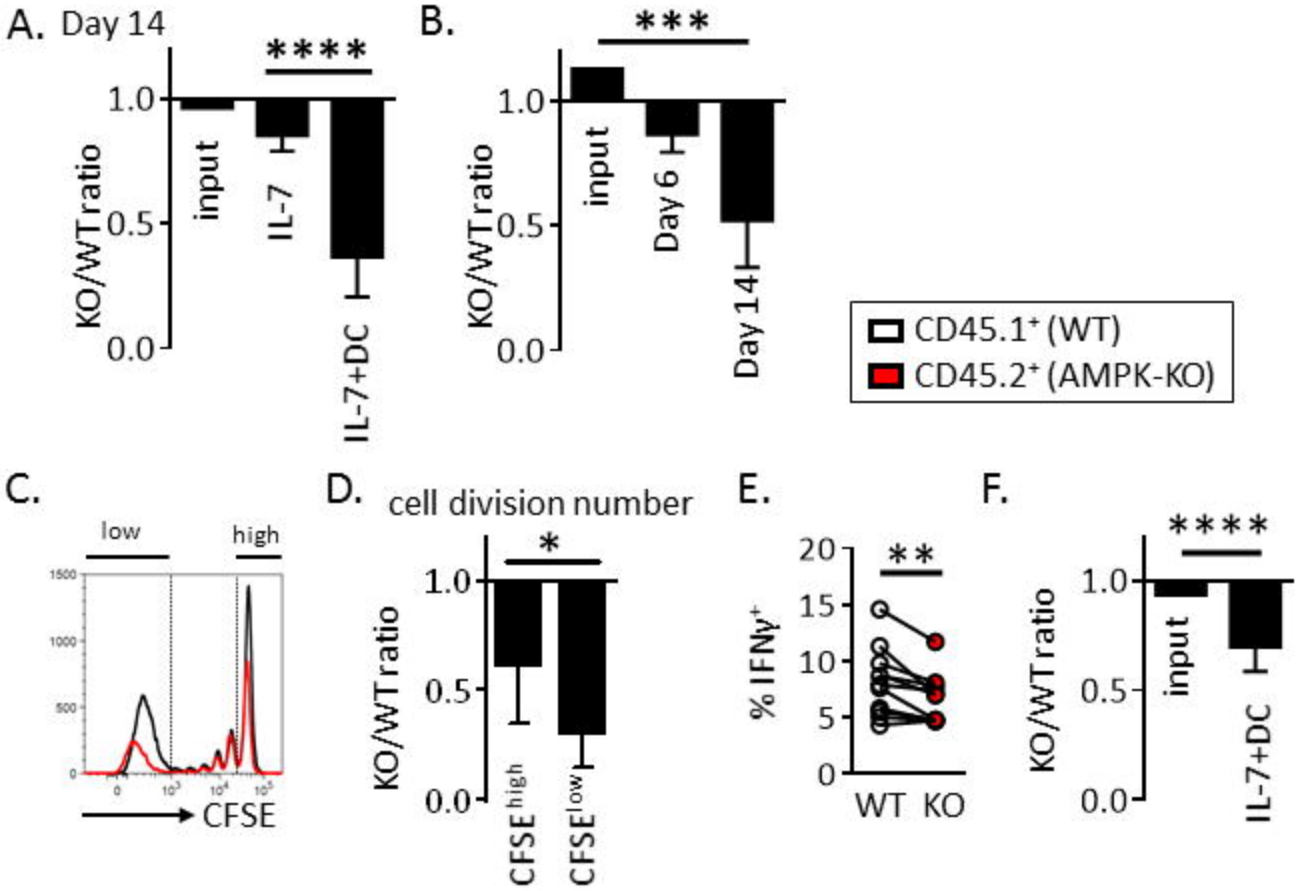
A.
Day 14
****
1.0
0.5
0.0
KO/WT ratio
input
IL-7
IL-7+DC
B.
***
1.0
0.5
0.0
KO/WT ratio
input
Day 6
Day 14
CD45.1+ (WT)
CD45.2+ (AMPK-KO)
C.
low
high
1500
1000
500
0
CFSE
D.
cell division number
*
1.0
0.5
0.0
KO/WT ratio
CFSE high
CFSE low
E.
**
20
15
10
5
0
% IFNγ+
WT
KO
F.
****
1.0
0.5
0.0
KO/WT ratio
input
IL-7+DC

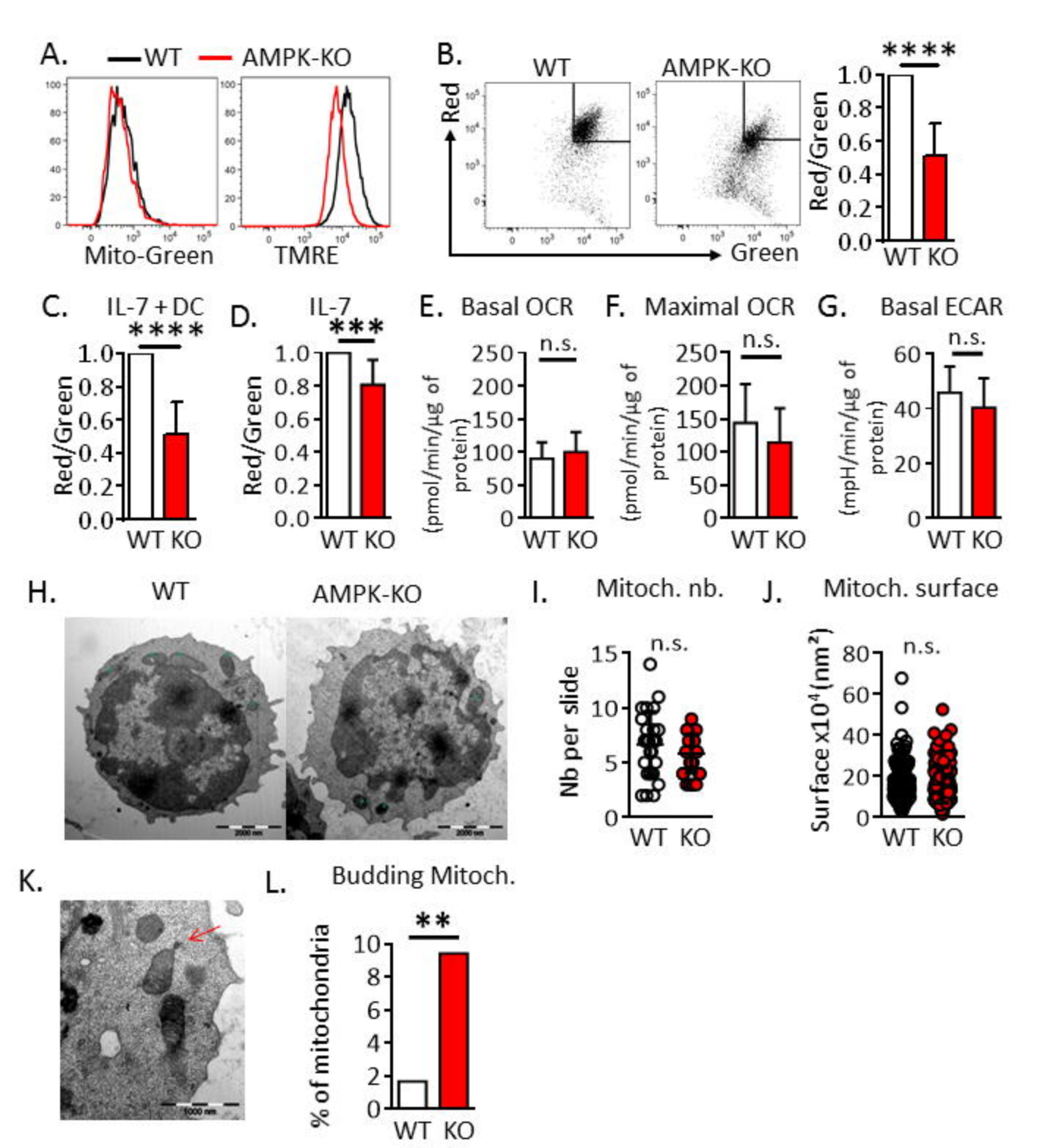
A.
WT
AMPK-KO
Mito-Green
TMRE
B.
WT
AMPK-KO
Red
Green
****
Red/Green
WT KO
C.
IL-7 + DC
****
Red/Green
WT KO
D.
IL-7
***
Red/Green
WT KO
E.
Basal OCR
n.s.
(pmol/min/µg of protein)
WT KO
F.
Maximal OCR
n.s.
(pmol/min/µg of protein)
WT KO
G.
Basal ECAR
n.s.
(mpH/min/µg of protein)
WT KO
H.
WT
AMPK-KO
I.
Mitoch. nb.
n.s.
Nb per slide
WT KO
J.
Mitoch. surface
n.s.
Surface x10⁴(nm²)
WT KO
K.
L.
Budding Mitoch.
**
% of mitochondria
WT KO

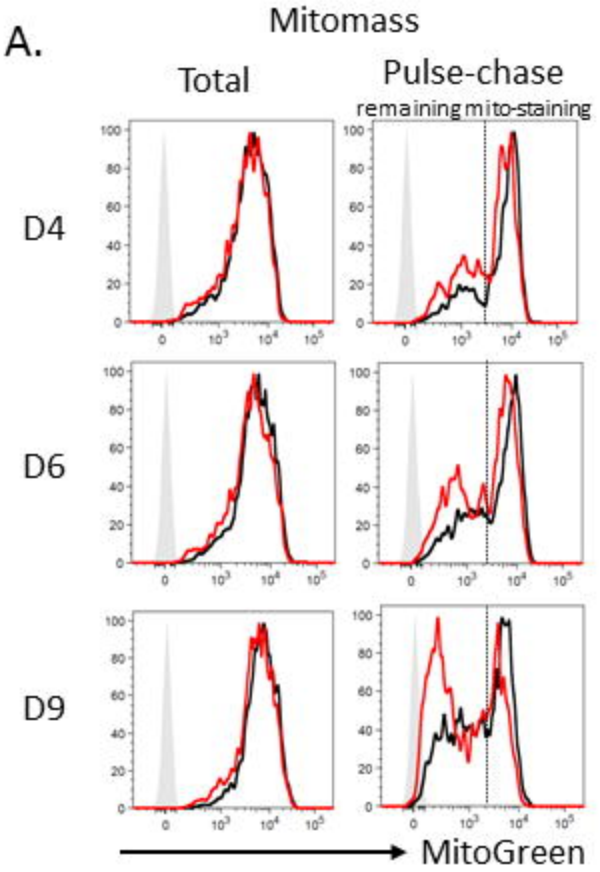
A.
Mitomass
Total
Pulse-chase
remaining mito-staining
D4
D6
D9
MitoGreen

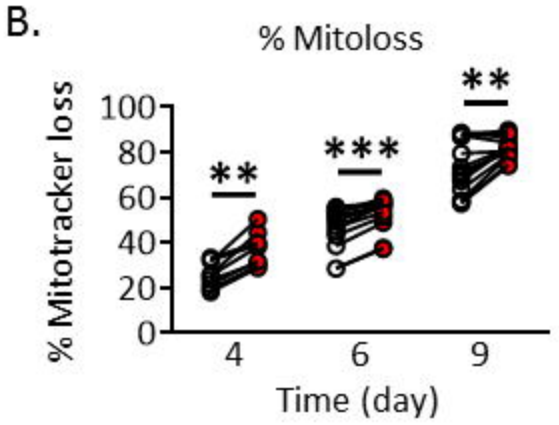
B.
% Mitoloss
% Mitotracker loss
100
80
60
40
20
0
**
***
**
4
6
9
Time (day)

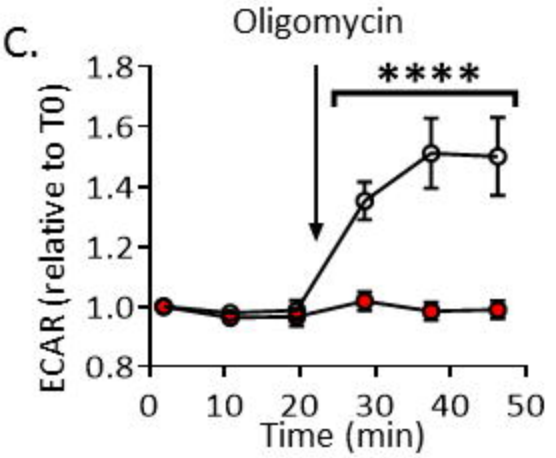
C.
Oligomycin
****
ECAR (relative to T0)
1.8
1.6
1.4
1.2
1.0
0.8
0
10
20
30
40
50
Time (min)

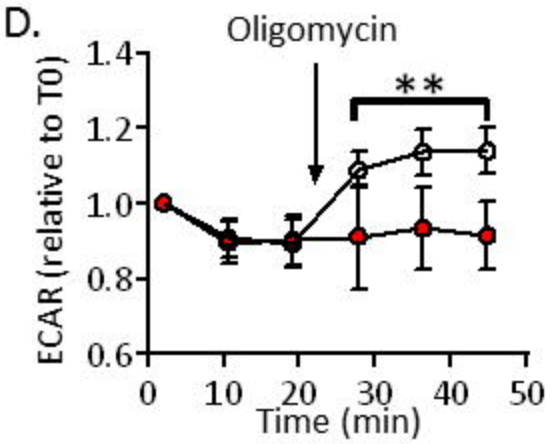
D.
Oligomycin
**
ECAR (relative to T0)
1.4
1.2
1.0
0.8
0.6
0
10
20
30
40
50
Time (min)

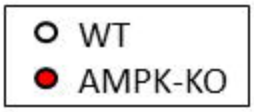
WT
AMPK-KO

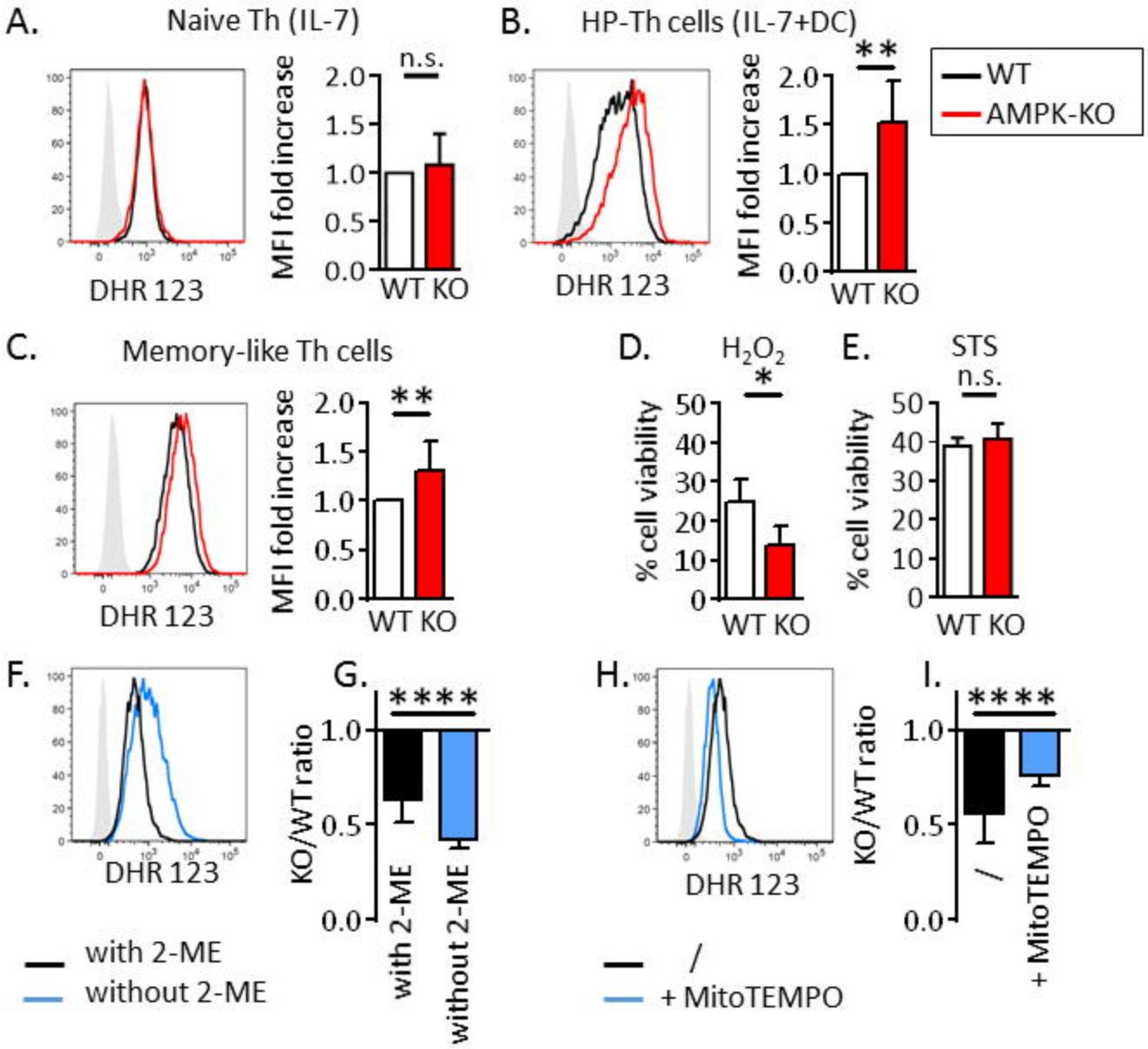
A.
Naive Th (IL-7)
DHR 123
MFI fold increase
n.s.
WT KO
B.
HP-Th cells (IL-7+DC)
DHR 123
MFI fold increase
**
WT KO
WT
AMPK-KO
C.
Memory-like Th cells
DHR 123
MFI fold increase
**
WT KO
D.
H2O2
*
% cell viability
WT KO
E.
STS
n.s.
% cell viability
WT KO
F.
DHR 123
with 2-ME
without 2-ME
G.
****
KO/WT ratio
with 2-ME
without 2-ME
H.
DHR 123
/
+ MitoTEMPO
I.
****
KO/WT ratio
/
+ MitoTEMPO